


High Gain Boost Converter Fed Single-Phase Sine Pulse Width Modulated Inverter

Rahul Kotana*, SK Hima Bindu*, Ramanjaneya Reddy Udumula*, Srikanth Goud B**,

*Department of Electrical and Electronics Engineering, SRM University – AP, Neerukonda, Andhra Pradesh, India-522503

** Department of Electrical and Electronics Engineering, Anurag University, Venkatapur, Ghatkesar, Telangana, India-500088

(kotana_phani@srmmap.edu.in, shaik_himabindu@srmmap.edu.in, urreddy89@gmail.com, srikanth.b@anuraghyd.ac.in)

‡ Corresponding Author: Ramanjaneya Reddy Udumula, SRM University – AP

urreddy89@gmail.com

Received: 17.02.2022 Accepted: 27.03.2022

Abstract- A high gain boost converter fed single-phase voltage source inverter with its control for DC to AC power conversion in uninterrupted power supply and renewable energy applications is presented in this paper. The conventional DC-DC boost converter with a coupled inductor and switched capacitor is utilized to obtain high gain. Further, the output voltage of the inverter is controlled by sinusoidal pulse width modulation technique. The detailed design and analysis of high gain boost converter fed single-phase voltage source inverter is also presented. The sine pulse width modulation control scheme for the voltage source inverter is developed and presented. In order to validate the high gain boost converter fed single-phase voltage source inverter, the simulation model is developed in LTspice software environment and results are validated. The results show high gain boost converter achieves a gain of about 10 and the single-phase voltage source inverter is able to provide a rms voltage of 228 V without using the step-up transformer. The total harmonic distortion of output current is found to be reduced below 4%. Further, the results obtained are found to be in close agreement with theoretical values.

Keywords- Boost converter, coupled inductor, switched capacitor, voltage source inverter, sine pulse width modulation.

1. Introduction

Energy is an essential factor for the functioning and economic development of the industrialized world. It plays a key role in our day-to-day life and on the other hand energy management has become critical factor for our successive economic prosperity. The energy consumption process frequently needs either DC-AC conversion or AC-DC conversion. The DC-AC conversion finds its major application in uninterrupted power supply (UPS) and renewable energy (RE). In order to supply during power outages, most UPS systems use batteries, usually lead acid, as storage mechanism. The battery is supposed to provide the backup in the absence of the grid supply. However, the voltage provided by the battery alone may not be enough to provide the backup. At first, the battery output power which is DC needs to be converted to AC with the help of an inverter. Apparently, the output of inverter needs to be step up with the help of step-up transformer to achieve an output of 220V 50Hz [1]. An alternative approach to the same process is by using a

power electronic converter called DC-DC boost converter. The boost converters are used in many applications, including photovoltaic systems, UPS, and fuel cell (FC) systems [2]. The standard DC-DC boost converter cannot provide a high gain. As it has been studied in the literature, when the voltage gain is high the efficiency of boost converter reduces. Reason being the losses in the intrinsic resistors of the converter increase when the duty cycle increases, which compromises the performance of the converter [3]-[4]. To overcome this limitation, high gain converter can be used to achieve higher gain [5]-[6]. AC output can be achieved with the help of inverter. Also, DC-AC conversion finds its application in RE systems. In such applications like solar photo voltaic (PV) systems, the DC output power from PV needs to be converted to AC power [7]. Many countries around the world are now looking at the installation of PV power plants and the number of power plants increased considerably, which resulted in an increased proportion of alternative energy sources for the generation of electricity [8]. One of the important tasks in PV generation is the DC-AC conversion method. But before AC

conversion, there is a need of stepping up of PV output DC power. With an abundance of solar power, at disposal and major modification in the area of power electronic conversion devices, DC grid can be used for a household in a distant or rural area to power, utilizing Solar PV [9]. Fig. 1 (a) and Fig. 1 (b) illustrates the DC-AC conversion adopted in [1] and [7] respectively.

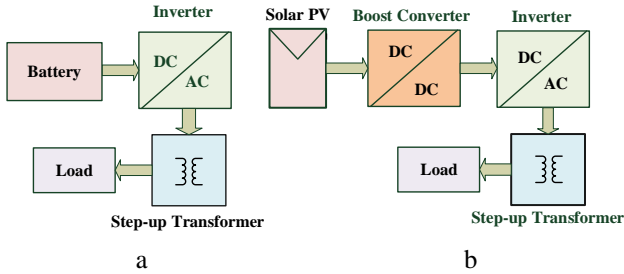


Figure. 1 Block diagram of DC-AC conversion system

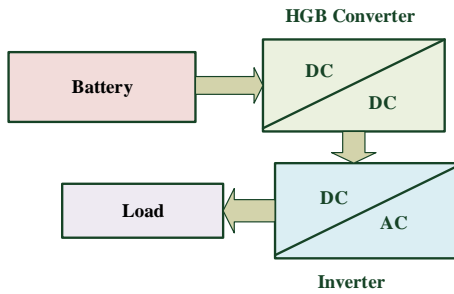


Figure. 2 Block diagram of DC-AC conversion based on HGB converter fed single phase VSI.

The boosting of battery voltage can be achieved with the help of standard boost converter as shown in Fig. 1(b), or by using a battery capable of supplying higher voltage and a step-up transformer as shown in Fig. 1(a). High power batteries and step-up transformers can be eliminated if a high gain boost (HGB) converter is used instead of a standard boost converter. Few authors have proposed, different types of non-standard boost converter configurations such as coupled inductor [10] and quadratic boost switched capacitor (SC) [11] are proposed for achieving high gain. However, when those configurations are used there is a compromise between gain and switching loss. Further several authors proposed boost converter fed DC-AC conversion system [13]-[21]. The HGB converter fed DC-AC conversion system is presented in this paper which eliminates the step-up transformer. The circuit configuration of proposed work is depicted in Fig. 2.

The paper is organized as follows; Section 2 describes the circuit configuration and operation followed by the introduction in Section 1. Simulation and result analysis are presented in the Section 3. Finally, in Section 4 the paper is concluded.

2. Circuit Configuration and Operation

The proposed DC-AC converter configuration is shown in the Fig. 3. The HGB converter configuration consists of a combination of two voltage gain techniques namely, coupled inductor (CI) and switched capacitor (SC). The voltage source inverter (VSI) converts the boosted DC voltage to AC voltage.

The sinusoidal pulse width modulation (SPWM) technique can be used to control the switches S_1, S_2, S_3 and S_4 of the inverter.

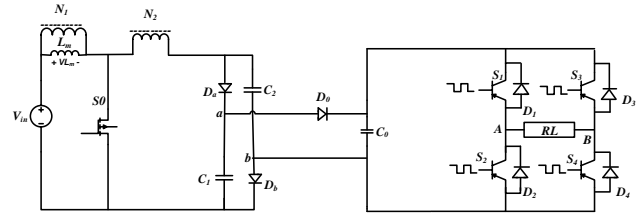
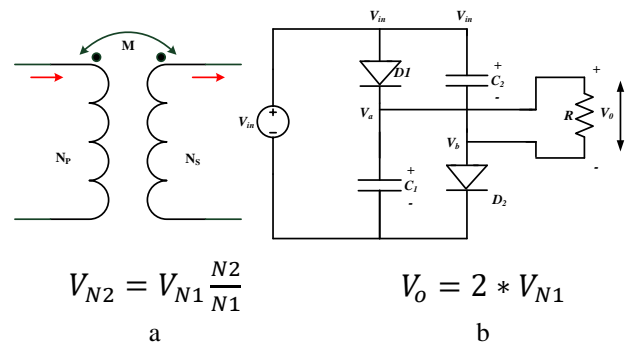


Figure. 3 Circuit diagrams of proposed DC-AC conversion system

The design and analysis of the proposed work is divided into two major parts such as HGB converter and voltage source inverter. The equivalent representation of CI model and SC model are depicted in Fig.4 (a) and Fig. 4(b) respectively. From Fig. 4 (a) it can be understood that the secondary voltage equal to turns ratio (N) times the primary voltage and from Fig. 4 (b) the output voltage of switched capacitor is two times the input voltage.



$$V_{N2} = V_{N1} \frac{N2}{N1} \qquad V_o = 2 * V_{N1}$$

Figure. 4 Voltage gain techniques. (a) coupled inductor. (b) switched capacitor

2.1. Analysis of High Gain DC-DC Boost Converter

Figure. 5 shows the circuit configuration of a HGB converter based on the voltage gain techniques such as CI and SC. The configuration of a HGB converter offers a gain approximately 10-12 times as compared to conventional boost converter [5]. The converter is designed to operate in continuous conduction mode (CCM); therefore, it has two modes of operations which are explained as follows.

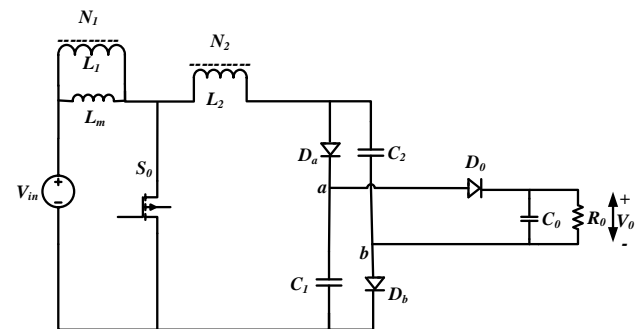


Figure. 5 Circuit Diagram of HGB Converter

Mode-1: ($0 \leq t < DT$) [see Fig. 6 (a)]:

During mode-1 time interval ($0 \leq t < DT$), the switch (S_1) conducts, while diodes D_1 and D_2 are reverse biased. The equivalent circuit of HGB converter in mode-1 is depicted in Fig. 6 (a). During this interval, the voltage across the magnetizing inductance (L_m) is equal to the DC input voltage, therefore, the current through magnetizing inductance (i_{Lm}) increases linearly. As the diodes D_1 and D_2 are in off state, the power to the load is supplied by the capacitors C_1 and C_2 . Fig. 6 (a) shows the path of current flowing in the circuit. The voltage across magnetizing inductance (L_m) can be found by applying kirchhoff's voltage law (KVL), as follows:

$$V_{Lm} = V_{in} \tag{1}$$

$$L_m \frac{di_{Lm}}{dt} = V_{in} \Rightarrow \Delta i_{Lm} = \frac{V_{in}}{L_m} DT \tag{2}$$

From Fig. 6(a) it can be seen that the current flowing through the capacitor C_2 is equal to the current through the secondary winding (i_{N2}) of the CI i.e., i_{N2} is equal to i_{C2} . The transformer turns ratio can be defined in terms of CI currents as follows.

$$N = \frac{i_{N1}}{i_{N2}} \tag{3}$$

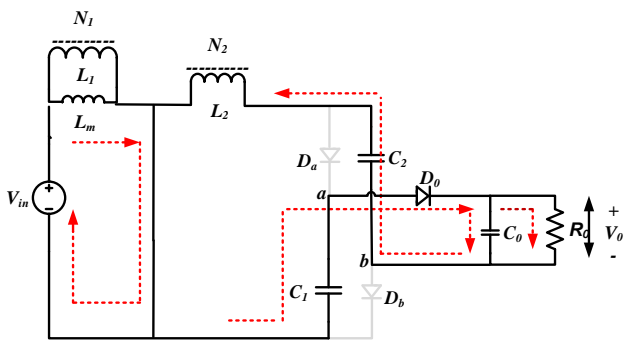


Figure. 6 (a) Equivalent circuit of HGB converter when switch S_1 is closed

By applying kirchhoff's current law (KCL),

$$i_{N2} = i_{C2} = \frac{-i_{Lm}}{(1+N)} \tag{4}$$

Applying KCL at node between diode (D_0), output capacitor (C_0) and load (R_0), the following expressions are obtained,

$$i_{C1} + i_{C0} = \frac{V_0}{R} \tag{5}$$

$$i_{C1} = i_{C2} \tag{6}$$

Mode-2: ($DT < t \leq T$) [see Fig. 6 (b)]:

During mode-2 in the interval ($DT < t \leq T$), the switch (S_1) is turned-off, while diodes D_1 and D_2 are forward biased. The equivalent circuit of HGB converter during the switch is open is depicted in Fig. 6 (b). During this instant of time, the voltage across the magnetizing inductance L_m is determined by the DC input voltage (V_{in}) and voltages across the secondary winding

(V_{N2}) and the capacitor voltage (V_{C1}) which results in the decaying of i_{Lm} . The diode (D_0) is reverse biased during this interval and the power to load is supplied by the charge stored in the C_0 . The current directions are represented in Fig. 6 (b). By applying KVL, the voltage across L_m can be expressed as follows.

$$V_{Lm} = V_{in} - V_{N1}(N) - V_{C1} \tag{7}$$

From the Fig. 6 (b), it can be found that, $V_{Lm} = V_{N1}$, by simplifying eq. (7) the voltage across L_m can be obtained as follows;

$$V_{Lm} = \frac{V_{in}-V_{C1}}{(1+N)} \Rightarrow \Delta i_{Lm(open)} = \frac{V_{in}-V_{C1}}{(1+N)L_m} (1-D)T \tag{8}$$

The current flowing through the winding N_2 is the input current (i_{in}) and the switched capacitors C_1 and C_2 shares the current i_{in} equally and equal to $i_{in}/2$. Now, the current through winding N_1 will be N times the input current i_{in} .

By applying KCL,

$$i_{Lm} = i_{in} + Ni_{in} \tag{9}$$

By rearranging the eq. (9)

$$i_{in} = \frac{i_{Lm}}{(N+1)} \tag{10}$$

The current through the switched capacitors is expressed as follows

$$i_{C1} = i_{C2} = \frac{i_{Lm}}{2(N+1)} \tag{11}$$

Since the average voltage across L_m is zero over a switching period (T), by using eq. (1) and eq. (7)

$$\frac{V_{in}-V_{C1}}{(1+N)} (1-D)T + V_{in}DT = 0 \tag{12}$$

By simplifying the eq. (12) the voltage across capacitor C_1 can be obtained as

$$V_{C1} = \frac{(1+ND)V_{in}}{(1-D)} \tag{13}$$

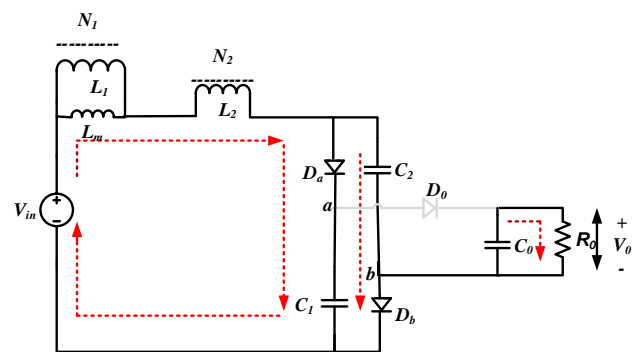


Figure. 6 (b) Equivalent circuit when switch S_1 is open

Note that, as V_{C1} and V_{C2} are the voltages across the capacitors C_1 and C_2 which are connected to the same node, thus both are equal. Thus, from the Fig. 3, voltage at point a is given by the

sum of V_{C1} and V_{N2} and, voltage at point b is V_{C2} . Now, output voltage is given by,

$$V_0 = V_a + V_b \quad (14)$$

By simplifying eq. (14) the output voltage can be obtained as follows

$$V_0 = V_{in} \left[\frac{2+ND+N}{1-D} \right] \quad (15)$$

The gain of HGB converter is given by the expression below,

$$\frac{V_0}{V_{in}} = \left[\frac{2+ND+N}{1-D} \right] \quad (16)$$

The switched capacitors C_1 , C_2 and output capacitor C_0 can be found from the equations below:

$$C_1 = C_2 = \frac{i_{Lm}(1-D)}{2(N+1)f\Delta V_c} \quad (17)$$

$$C_0 = \frac{i_0(1-D)}{f\Delta V_0} \quad (18)$$

2.2. Design considerations of high gain boost converter

A 36 V DC input voltage is taken into consideration to validate the HGB converter. The voltage and current through the output terminals of HGB converter is 360 V and 3.6 A, respectively. The HGB converter is operated at a switching frequency of 50 kHz. By considering the inductor ripple current as 20%, the value of L_m can be calculated from the following expression,

$$L_m = \frac{DV_{in}}{f_s \Delta I_{Lm}} = 265.214 \mu H \quad (19)$$

Inductor with N_1 turns will produce a total flux Φ_t . Note that, flux Φ_t is a combination of magnetizing flux Φ_m and leakage flux Φ_{lk} . Leakage flux is very less compared to the magnetizing flux. The expression for self-inductance of a coil is given by,

$$L_1 = \frac{N_1 \Phi_t}{i_1} = \frac{N_1 \Phi_m}{i_1} + \frac{N_1 \Phi_{lk}}{i_1} \quad (20)$$

$$L_1 = L_m + L_{lk} \Rightarrow L_1 \cong L_m = 265.214 \mu H \quad (21)$$

The secondary inductance can be obtained by using the following relation,

$$\left(\frac{N_2}{N_1} \right)^2 = \frac{L_2}{L_1} \Rightarrow L_2 = 2.386 mH \quad (22)$$

Assuming 100% coupling coefficient ($k=1$), the mutual inductance can be obtained by using the following expression,

$$M = \sqrt{L_1 L_2} = 795.4 \mu H \quad (23)$$

By using eqn. (13), the voltage across switched capacitors C_1 and C_2 is obtained as follows,

$$V_{C1} = V_{C2} = \frac{(1+ND)V_{in}}{(1-D)} = 125.755 V \quad (24)$$

The values of switched capacitors C_1 and C_2 and output capacitor C_0 is obtained as follows,

$$C_1 = C_2 = \frac{(1-D)i_{Lm}}{(2N+2)(f_s)\Delta V_c} = 1.2 \mu F \quad (25)$$

$$C_0 = \frac{(1-D)i_0}{f_s \Delta V_0} = 613 \mu F \quad (26)$$

2.3. Analysis of single-phase voltage source inverter

The circuit diagram of a single-phase VSI is depicted in Fig. 7. A single-phase VSI converts DC to AC. The output of inverter is more like a square wave output except that it has one more level i.e., before switching positive or negative the output goes to zero volts. A pure or true sine wave inverter converts the DC into near perfect AC output [12]. Fig. 3 shows that the DC input to the inverter is fed from the output of the HGB converter. The AC output is obtained by turning ON and OFF the switches in the right sequence. Pulse width modulation (PWM) strategy is used to control the semiconductor devices [13].

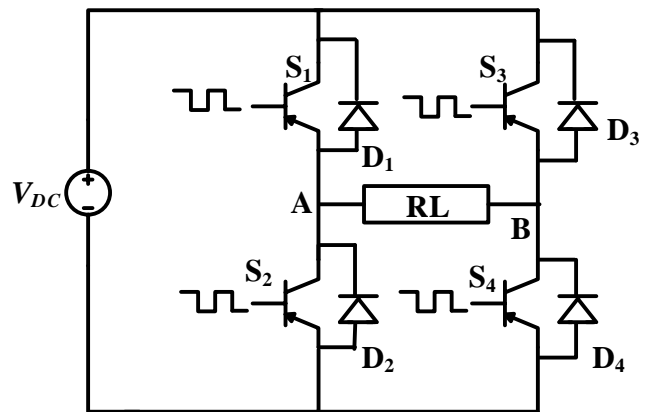


Figure. 7 Single phase voltage source inverter

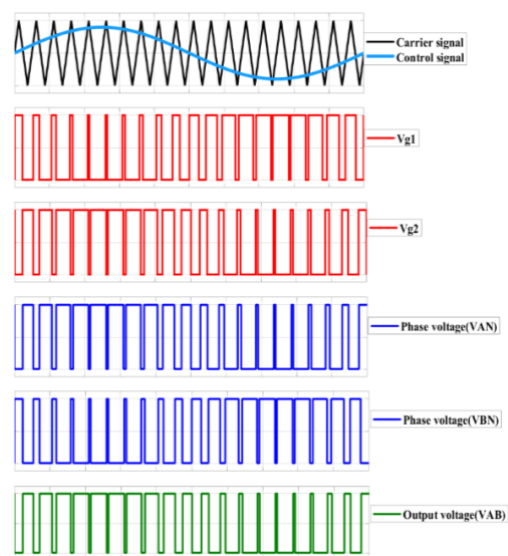


Figure. 8 Ideal waveforms of bipolar modulation scheme [14]

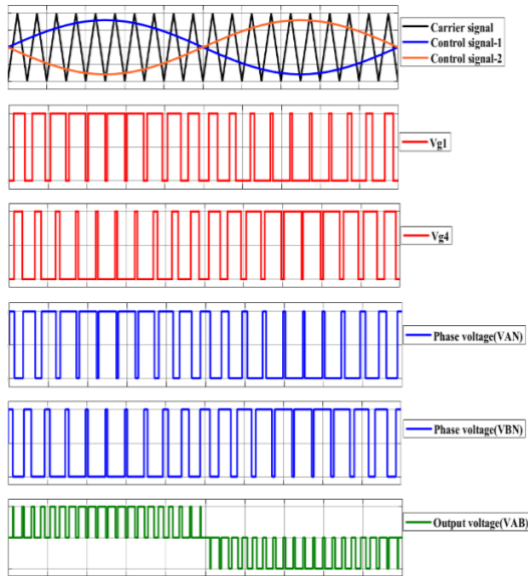


Figure. 9 Ideal waveforms of unipolar modulation scheme [14]

The switching sequence is such that, two switches, each from either leg operates for $T/2$ interval. The diodes will be operating, as the circuit is intended to be connected with RL load. Each combination of switches will be operating for $T/2$ interval. The fig. 8, shows the output of the inverter is not sinusoidal but a square wave. The total harmonic distortion (THD) of a square wave is about 48% [16] which is very high resulting in lower power factor [15]. As low power factor is undesirable, square wave must be avoided. In order to reduce the harmonics, pulse width modulation (PWM) technique is used. The PWM is obtained by the varying the duty cycle of a periodic signal. For industrial and household applications, sinusoidal waveforms are best suited because they are having low levels of distortions and lower order harmonics [16]. Thus, in the proposed work SPWM is adopted. Bipolar and unipolar SPWM are the two types of sinusoidal PWM techniques. In bipolar SPWM, control signal is a sinusoidal wave and carrier signal is a triangular wave. By comparing the control signal with the carrier signal the output pulses are generated. The waveforms of bipolar SPWM scheme are shown in the Fig. 8. In a circuit, the operation of switches is different if unipolar modulation is provided as shown in Fig. 9. The switches are operated complementary based on the triangular wave. Furthermore, the sinusoidal control voltages in both the legs are opposite to each other. A three-level voltage output is produced by unipolar SPWM which is either 0 or $\pm V_{dc}$. For unipolar modulation two control signals and one reference signal are required. The two control signals are sinusoidal signals with 1800 phase delay. The carrier wave is triangular signal. if control-1 \geq carrier, S_1 is ON else S_4 is ON. If control-2 \geq carrier; S_3 is ON else S_2 is ON. It shows that, no two switches of the same leg are operated at the same instant of time. Thus, the two switches of the same leg will not conduct simultaneously. Fig. 9 shows the waveforms for unipolar SPWM. In case unipolar modulation is implemented in a circuit, the connection function is different in both

branches. Given that the switches must be complementary in performance, both branches of the bridge are related by the triangular voltage. Furthermore, the sinusoidal control voltage is opposite in sign in both legs. The output of unipolar SPWM has three levels $+V_{dc}$, 0, $-V_{dc}$. The output of unipolar SPWM is more accurate than bipolar modulation [17].

3. Simulation Results and Analysis

To validate the SPWM control scheme with DC-AC conversion system, a detailed analysis and simulation of the circuit in Fig. 2 are performed by using LTspice simulation environment. Table.1 illustrates the specifications and design parameters used for simulation analysis of proposed system.

TABLE.1 Specifications used in simulation of proposed DC-AC conversion system

Design Parameter	Rating
DC Input Voltage (V_{in})	36V
Switching Frequency (f_s)	50 kHz
Duty Ratio (D)	0.384596
Switched Capacitances (C_1 & C_2)	1.2 μ F
Output Capacitance (C_o)	612 μ F
Inductance (L_1)	265.2 μ H
Inductance (L_2)	2.386 mH
Carrier Frequency (f_r)	1 kHz
RL load	R= 50 Ω & L= 50 μ H

Fig. 10 shows the simulation results, input voltage (V_{in}) and output voltage (V_o) of HGB converter. From Fig. 10 the output voltage of HGB converter is found as 360 V which satisfies the designed value. The HGB converter results in high gain as compared with the conventional boost converter. Therefore, HGB converter eliminates the use of step-up transformer along with single phase voltage source inverter. Whereas the conventional boost converter fed voltage source inverter requires a step-up transformer in order to obtain the 220 V rms output voltage.

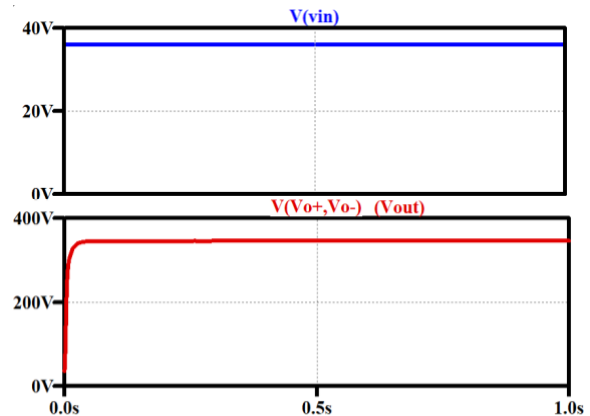


Figure. 10 Simulation waveforms of input voltage (V_{in}) and output voltage (V_o) of HGB converter

The Fig. 11 shows the waveforms of switched capacitors voltages (V_{C1} & V_{C2}) and switched capacitor currents (I_{C1} & I_{C2}) of HGB converter obtained by simulation. It clearly indicates the voltage across switched capacitors are equal and abide by the designed values. Fig.12 depicts the waveforms of magnetizing inductor current (i_{Lm}) and magnetizing inductor voltage (V_{Lm}) obtained by simulation. The magnetizing inductor current waveform in Fig. 12 shows the operation of HGB converter is in CCM.

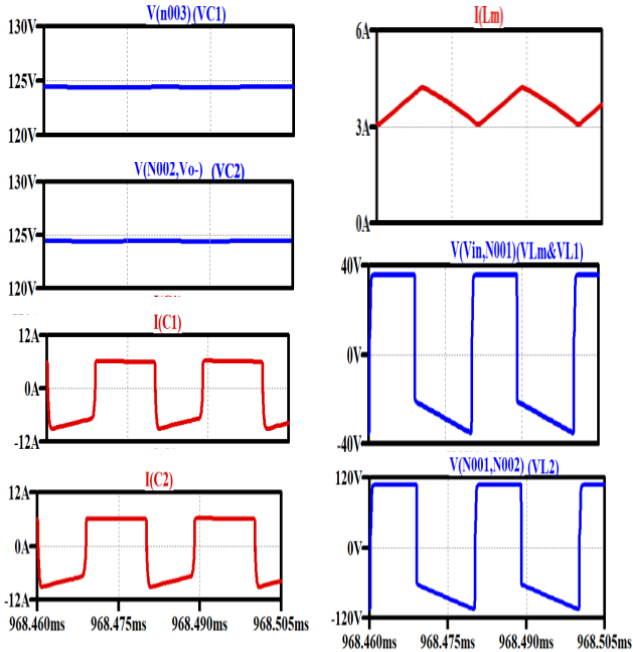


Figure. 11 Simulation waveforms V_{C1} , V_{C2} , I_{C1} and I_{C2} of HGB converter

Figure. 12 Simulation waveforms i_{Lm} , V_{Lm} , i_{L1} and i_{L2} of HGB converter.

Fig. 13 shows the simulation results of unipolar SPWM control scheme which is adopted to control the voltage source inverter (VSI). It indicates that by using unipolar control scheme the switching pulses for the VSI is generated by comparing the reference and control signals as discussed in section 2.3. From the gating signals it can be observed that the switching pulses are complementary, which results in the elimination of short circuit of a leg at any point of time. Figure.14 shows the simulation results of proposed HGB converter for the input of 36V DC, a rms output voltage of 228V AC is obtained without using a transformer unlike as done in [1]. The output current and THD waveform of VSI is shown in fig. 15 and total harmonic distortion (THD) of the output waveform found to be below 4%, which is less compared to the unmodulated square wave output of the inverter which was 48% [18].

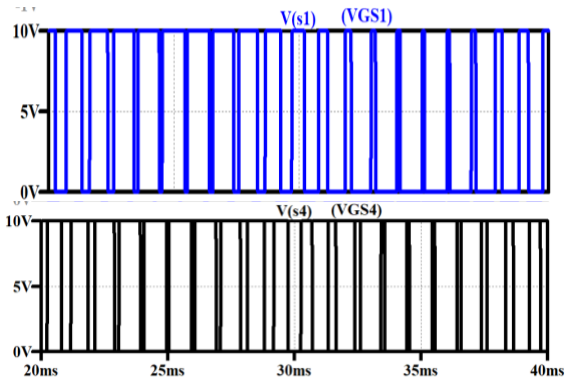
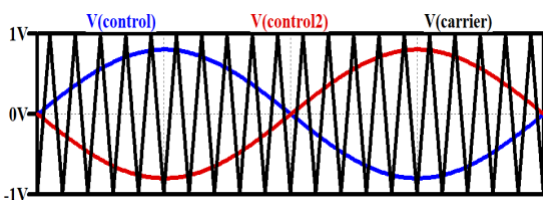


Figure. 13 Simulation results of single phase SPWM inverter

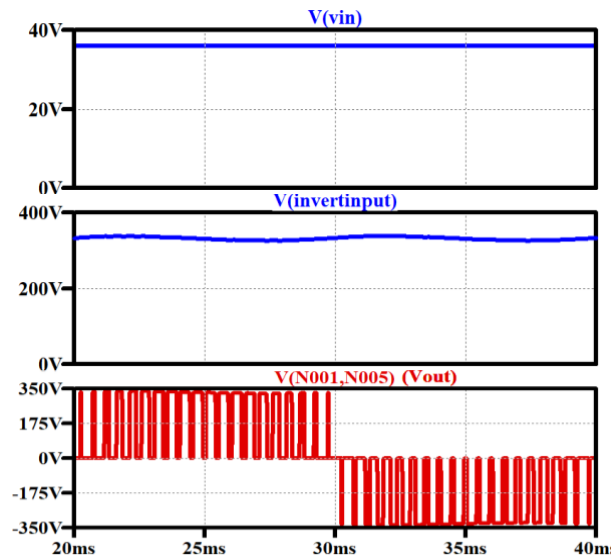


Figure. 14 Simulation results of the DC-AC conversion system proposed

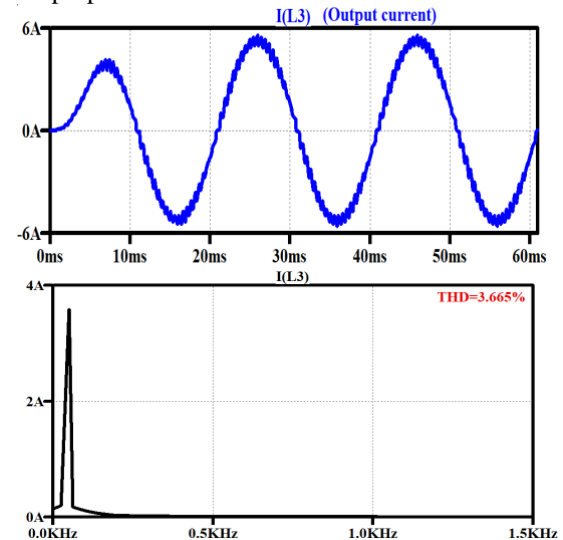


Figure. 15 Total harmonic distortion of output current.

TABLE II Comparative study of proposed HGB converter with other works in the literature

	Boost Converter	[10]	[11]	HGB Converter
MOSFETS	1	1	1	1
Diodes	1	2	5	3
Inductors	1	3	2	3
Capacitors	1	2	4	3
Component count	4	8	12	10
Output Ports	1	1	1	1
Turns Ratio	-	N	-	N
Gain	$\frac{1}{(1-D)}$	$\frac{ND+1}{1-D}$	$\frac{2}{(1-D)^2}$	$\frac{2+ND+N}{1-D}$

Table II depicts the comparative analysis of different configurations of boost converter. For the required gain of 10, the converter based on switched capacitor and coupled inductor can achieve the gain at a duty cycle (D) of 0.36 and with turns ratio (N) of 3. Whereas coupled inductor configuration will have D as 0.7. High duty cycle will result in higher switching loss, which affects the efficiency. On the other hand, conventional boost converter and switched capacitor configuration can never achieve a gain of 10. Considering all the above, HGB converter is adapted in the work.

TABLE III Comparative study of proposed DC-AC conversion with other work in the literature

Parameter	Panneerselvam et al. [7]	Proposed DC-AC conversion
DC-DC boost converter	Yes	Yes
Gain	1/1-D	(2+ND+N)/(1-D)
Converter type	Standard boost converter	HGB converter
Inverter	Yes	Yes
Transformer	Yes	No
Conversion steps	3	2

The comparative study of proposed high gain boost converter fed single-phase sine pulse width modulated inverter with similar topology is depicted in Table III. From comparative analysis it clearly indicates that the proposed work eliminates the use of transformer by using high gain boost converter which results in reduction of the overall size and also the conversion stages is reduced from three to two, resulted in increases the efficiency

4. Conclusion

This work proposes an DC-AC conversion method based on HGB converter fed single-phase SPWM inverter. The DC-AC converters have wide range of applications. The proposed model is best suited when a low voltage DC supply is available, and a standard 228V AC output is needed to deliver the load. The design, analysis and simulation of HGB converter is presented and the simulation results are found in agreement with designed values. The proposed HGB converter has a gain value of about 10, which is very high as

compared with conventional boost converter topologies. A unipolar SPWM control scheme is developed in LTspice to control the single phase VSI. The simulation results of complete DC-AC conversion system are in close agreement with the design parameters. Further, the total harmonic distortion of output current waveform is around 4% which is well below the international standards. In addition, the complete model consisting of both HGB converter and single phase VSI are successfully simulated for an input of 36V DC and produced a rms output voltage of 228 V.

References

- [1] ALBU, Răzvan-Daniel & Tepelea, L. & Popențiu-Vlădicescu, Florin, High Reliability Uninterruptible Power Supply, Journal of Electrical and Electronics Engineering, Vol. 3, Jan 2010.
- [2] P. Mazidi, G. N. Baltas, M. Eliassi and P. Rodríguez, A Model for Flexibility Analysis of RESS with Electric Energy Storage and Reserve, 2018 7th International Conference on Renewable Energy Research and Applications (ICRERA), 2018, pp. 1004-1009.
- [3] A. M. S. S. Andrade, L. Schuch and M. L. da Silva Martins, Analysis and Design of High- Efficiency Hybrid High Step-Up DC-DC Converter for Distributed PV Generation Systems, IEEE Transection on Industrial Electronics, vol. 66 (5), pp. 3860-3868, May 2018.
- [4] A. Benyamina and S. Moulahoum, Real time implementation of unity power factor correction converter based on fuzzy logic, 2016 International Smart Grid Workshop and Certificate Program (ISGWCP), 2016, pp. 1-4.
- [5] H. J. Hoch, T. M. K. Faistel, M. M. da Silva, A. M. S. S. Andrade and M. L. d. S. Martins, High Voltage Gain DC-DC Converter based on a Simple Configuration of Switched Capacitor and Coupled Inductor, IEEE 15th Brazilian Power Electronics Conference and 5th IEEE Southern Power Electronics Conference, pp. 1-6, 2019.
- [6] Y. Soufi, M. Bechouat and S. Kahla, Fuzzy controller design using particle swarm optimization for photovoltaic maximum power point tracking, 2016 International Smart Grid Workshop and Certificate Program (ISGWCP), 2016, pp. 1-6.
- [7] Panneerselvam, Priya & Subramaniam, Lavanya & Perumal, Vimala. Solar Energy Fed Single Phase Inverter Through Boost Converter. Vol. 3, 2014.
- [8] Al-Maamary, H.M.S.; Kazem, H.A.; Chaichan, M.T. Changing the energy profile of the GCC states: A review. *Int. J. Appl. Eng. Res.* 2016, *11*, 1980–1988.
- [9] G. Arunkumar, D. Elangovan, P. Sanjeevikumar, J.B.H Nielsen, Z. Leonowicz, P.K. Joseph, DC Grid for Domestic Electrification, *Energies*, Vol. 12, 2019, pp. 2157.
- [10] Felinto S. F. Silva, Antônio A. A Freitas, Sérgio Daher, Saulo C. Ximenes, Sarah K. A. Sousa, M. S. Edilson,

- High gain DC-DC boost converter with a coupling inductor, *2009 Brazilian Power Electronics Conference*, 2009, pp. 486-492.
- [11] D. Sivaraj and M. Arounassalame, High gain quadratic boost switched capacitor converter for photovoltaic applications, *2017 IEEE International Conference on Power, Control, Signals and Instrumentation Engineering (ICPCSI)*, 2017, pp. 1234-1239.
- [12] H. Jiang and A. Ekstrom, Multiterminal HVDC systems in urban areas of large cities, *IEEE Transaction on Power Delivery*, vol. 13 (4), Oct. 1998, pp. 1278 – 1284.
- [13] P. F. de Toledo, Feasibility of HVDC for city infeed, Royal Institute of Technology, Stockholm, Sweden, Licentiate Thesis, 2003.
- [14] J. Holtz, Pulse width modulation-a survey, *IEEE Transactions on Industrial Electronics*, vol.39, no.5, pp.410-420, Dec. 1992.
- [15] I. Colak, E. Kabalci, Developing a novel sinusoidal pulse width modulation (SPWM) technique to eliminate side band harmonics, *International Journal of Electrical Power & Energy System*, Volume 44, Issue 1, January 2013 – Elsevier, Pages 861–871.
- [16] Ned Mohan, Tore M. Undeland, William P. Robbins, *Power Electronics: Converters, Applications, and Design*, 1989. John Wiley & Sons, Inc.
- [17] V. Fernão Pires, J. F. Martins, D. Foito, Chen Hão, A Grid Connected Photovoltaic System with a Multilevel Inverter and a Le-Blanc Transformer, *International Journal of Renewable Energy Research (IJRER)*, Vitor Fernão Pires et al., Vol.2, No.1, 2012.
- [18] Blagouchine, Iaroslav & Moreau, Eric, Analytic Method for the Computation of the Total Harmonic Distortion by the Cauchy Method of Residues. *Communications, IEEE Transactions on*. 59. 2478-249.
- [19] Concettina Buccella, Maria Gabriella Cimatori, Carlo Cecati, Low-Frequency Harmonic Elimination Technique in Cascaded H-Bridges Multilevel Inverters for Renewable Energy Applications, *International Journal of Smart Grid*, Vol 3, No 1 (2019).
- [20] S. Vadi, F. B. Gürbüz, R. Bayindir and E. Hossain, Design and Simulation of a Grid Connected Wind Turbine with Permanent Magnet Synchronous Generator, *2020 8th International Conference on Smart Grid (icSmartGrid)*, 2020, pp. 169-175.
- [21] U Ramanjaneya Reddy and B. L. Narasimharaju, A Cost-Effective Zero-Voltage Switching Dual-Output LED Driver, *IEEE Transactions on Power Electronics*, vol. 32, no. 10, pp. 7941-7953, Oct. 2017.
- [22] Ramanjaneya Reddy U and Narasimharaju B. L, Unity power factor buck-boost LED driver for wide range of input voltage application, *2015 Annual IEEE India Conference (INDICON)*, 2015, pp. 1-6.